Cell Proliferation

Cell Prolif., 2010, **43**, 310–320 doi: 10.1111/j.1365-2184.2010.00676.x

In vitro ovine articular chondrocyte proliferation: experiments and modelling

L. Mancuso*, M. I. Liuzzo*, S. Fadda*, M. Pisu†, A. Cincotti*, M. Arras‡, G. La Nasa‡, A. Concas† and G. Cao*,†

**Dipartimento di Ingegneria Chimica e Materiali, Università degli Studi di Cagliari, Cagliari, Italy, †CRS4 (Center for Advanced Studies, Research and Development in Sardinia), Località Piscinamanna, Cagliari, Italy, and ‡Servizio di diagnostica citofluorimetrica e trattamento cellule staminali, Centro Trapianti di Midollo Osseo, Cagliari, Italy*

Received 14 *April* 2009; *revision accepted* 21 *September* 2009

Abstract

This study focuses on analysis of *in vitro* cultures of chondrocytes from ovine articular cartilage. Isolated cells were seeded in Petri dishes, then expanded to confluence and phenotypically characterized by flow cytometry. The sigmoidal temporal profile of total counts was obtained by classic haemocytometry and corresponding cell size distributions were measured electronically using a Coulter Counter. A mathematical model recently proposed (1) was adopted for quantitative interpretation of these experimental data. The model is based on a 1-D (that is, mass-structured), single-staged population balance approach capable of taking into account contact inhibition at confluence. The model's parameters were determined by fitting measured total cell counts and size distributions. Model reliability was verified by predicting cell proliferation counts and corresponding size distributions at culture times longer than those used when tuning the model's parameters. It was found that adoption of cell mass as the intrinsic characteristic of a growing chondrocyte population enables sigmoidal temporal profiles of total counts in the Petri dish, as well as cell size distributions at 'balanced growth', to be adequately predicted.

Introduction

Tissue engineering is a very promising technique for treating patients with damaged cartilage caused by arthritis, trauma or congenital abnormality (2,3). Articular cartilage consists of an extracellular matrix (ECM) that is synthesized by chondrocytes, which are the resident cells of the tissue (4). During natural cartilage formation, chondrocytes proliferate and secrete collagen and proteoglycans (mainly constituted by glycosaminoglycans, GAG). *In vitro* chondrogenesis, required for repairing tissue by transplantation, resembles the natural *in vivo* process since, by taking advantage of synthetic scaffold supports (polymers, hydrogels), cells may grow, proliferate and synthesize ECM in parallel with scaffold degradation (2). To maximize cell expansion and ECM production for treatment of human patients, understanding of corresponding growth kinetics during cell culture *in vitro* is needed. Investigation into intrinsic cell kinetics may be performed using a static culture system (that is, in Petri dishes). Interpretation and analysis of the corresponding experiments, which provide a clear contribution to understanding the complex biological mechanisms involved, may be achieved by means of suitable mathematical models (1). Only a limited number of studies, in which comparisons between experimental data and model results of chondrocyte/cartilage *in vitro* culture, have been reported, and are available in the literature. In particular, Obradovic *et al.* (5) modelled oxygen consumption and GAG (glycoaminoglycan) deposition by bovine chondrocytes superficially seeded on to 3-D polymeric scaffolds, and cultured in rotating bioreactors. While oxygen and GAG concentrations were simulated by means of transient diffusion/reaction material balance equations, proliferation of chondrocytes was evaluated only experimentally. Later, Wilson *et al.* (6) modelled transient cartilage culture in 3-D constructs by neglecting spatial distribution and chondrocytes' proliferation kinetics, while taking into account scaffold degradation. A steady-state 1-D diffusion/reaction model of oxygen consumption inside scaffolds was proposed by Zhou *et al.* (7), without taking into account ECM production and chondrocyte proliferation.

Two modelling approaches have been proposed so far for mathematical description of proliferation of

Correspondence: G. Cao, CRS4 (Center for Advanced Studies, Research and Development in Sardinia), Località Piscinamanna, Edificio 1, 09010 Pula, Cagliari, Italy. Tel.: +39 070 675 5058; Fax: +39 070 675 5057; E-mail: cao@visnu.dicm.unica.it and A. Cincotti, Dipartimento di Ingegneria Chimica e Materiali, Università degli Studi di Cagliari, Piazza d'Armi, 09123 Cagliari, Italy. Tel.: +39 070 675 5066; Fax: +39 070 675 5057; E-mail: cincotti@visnu.dicm.unica.it

chondrocytes. The first is based on the use of phenomenological equations such as exponential growth, logistic and gompertzian sigmoidal curves, which aim to correlate quantitatively lag, log and stationary phases naturally present in any growing population inside a batch, discontinuous environment such as cell expansion, performed in a Petri dish. The second, a more sophisticated modelling approach, known as Population Balance Equations (PBE), is based on experimental evidence that the temporal behaviour of distribution of some intrinsic property (age, size, mass, DNA content and more) of the cell population is able to describe the kinetics of the system under investigation, in a quantitative fashion.

While the first approach provides a rough but simple mathematical description of proliferation kinetics (8–10), PBE modelling may reach a very detailed but complex depiction of system behaviour, by considering age- versus size-based formulations (11–17), unstructured versus structured framework (18), mono- versus multi-staged population of cells (17,19,20) and even complex combinations of these (21). A selection of recent literature references on proliferating cultures, where comparisons between experimental data and model results have been given, is reported in Table 1. Quantitative interpretation of experimental data concerning stem cell expansion by means of a PBE model approach has been recently attempted (1). Following this approach, the authors (24–26) coupled the transient diffusion/reaction model, developed by Obradovic *et al.* (5) for the case of *in vitro* cartilage culture, with mathematical description of proliferation of chondrocytes, by means of a mass-structured population balance. Comparisons with experimental data taken from the literature were provided only in terms of reported ECM components' spatial distributions or temporal profiles and total cell count evolution. Thus, in these studies, the assumption that distribution of masses inside a growing population of chondrocytes may be adopted to simulate adequately cell proliferation was not completely verified, as comparisons with experimental data in terms of cell distributions were not available.

Here, the kinetics of ovine articular chondrocyte culture in a static system (Petri dish) has been addressed. The *ovine model* was chosen as the experimental cell system as it is more similar to equivalent *human* cells in terms of size and DNA than the classical *murine* model. *In vitro* culture of ovine chondrocytes has been the subject of several investigations. In particular, expansion of ovine chondrocytes has been evaluated for cartilage tissue engineering through comparison with human, porcine and equine models (27). The effect of growth factors on proliferation and de-differentiation of these cells seeded on to a PGA scaffold has also been analysed by Stewart *et al.* (28). In addition, proliferation rates of ovine primary chondrocytes from different anatomical locations (29), and of ovine chondrocytes derived from either bone marrow (30) or umbilical cord blood mesenchymal stem cells (31) have been evaluated. However, in all these studies, expansion rate of ovine chondrocytes has been investigated only experimentally, while here, a theoretical analysis has also been performed following the same approach proposed in our previous investigation (1).

Specifically, expansion kinetics was experimentally measured through classic haemocytometry by following the temporal evolution of total counts, while number distribution of cell sizes was estimated using an electronic Coulter Counter. Phenotypic characterization of cell

Table 1. Literature references related to proliferating cultures where comparison between experimental data and model results is presented

Mathematical modelling approach	Model system	Comparison with experimental data	Reference
PBE (age, multi-staged)	CHO and mouse-mouse hybridoma cell lines	Total cell count temporal profile	Abu-Absi and Srienc (14)
Exponential growth with cell loss	Muscle- derived stem cells	Total cell count temporal profile (fitting)	Deasy *et al.* (8)
PBE (DNA content, multi-staged)	Human cancer cell line	Distributions of DNA content (fitting)	Basse *et al.* (20)
PBE (mass, structured, multi-staged)	Hybridoma and animal cell lines	Total cell count, substrates, and products temporal profiles (fitting)	Sidoli *et al.* (18)
PBE (mass)	Human cancer cell lines	Total cell count, Tumour radius and mass temporal profiles (fitting)	Busini *et al.* (22)
PBE (volume, structured, multi-staged)	Myeloma cell line	Total cell count, substrates, products, and cell phase fractions temporal profiles (fitting); distributions of DNA content (qualitative comparison)	Liu *et al.* (21)
PBE (age, multi-staged)	Human leukaemia cells	Cell phase fractions temporal profiles (fitting)	Sherer *et al.* (17)
PBE (protein content, multi-staged)	Yeast	Distributions of protein content (qualitative comparison)	Hatzis and Porro (23) Cipollina *et al.* (15)
PBE (mass)	Sheep bone marrow mesenchymal stem cells	Total cell count (fitting)	Mancuso *et al.* (1)

lineage was performed by means of flow cytometry, to verify that cultured chondrocytes in a monolayer do not de-differentiate to fibroblast-like cells. Proliferation kinetics and cell size distribution were then simulated by adopting a mass-based PBE model approach proposed by Mancuso *et al.* (1), where growth, limited by contact inhibition as the population increased, was taken into account, under the assumption of excess nutrients and oxygen supply. To determine values for the unknown model parameters, the model was fitted to temporal evolution of experimental total cell counts (up to 8 days of culture time) and to cell size distributions (up to 4 days of culture time) reported in terms of histograms (cell number frequencies vs cells' diameter). Then, model reliability was verified by predicting cell proliferation and histogram size distributions, measured over longer culture time.

Materials and methods

Isolation of ovine chondrocytes

Chondrocyte cultures were prepared from ovine articular cartilage, which was dissected from joints of an 8-month-old lamb, obtained from a local slaughterhouse, and washed in culture medium (DMEM supplemented with 10% foetal calf serum, 2 mM glutamine, 100 U/ml penicillin, 100 mg/ml streptomycin, 2.5 mm/ml amphotericin B). Tissue was chopped into 1–4 mm fragments and washed three times again in culture medium. Previous medium was removed and the cartilage was gently shaken in fresh culture medium solution, with 1% pronase (Sigma, St Louis, MO, USA) for 2 h, followed by type 1A collagenase at concentration of 300 units/ml (Type 1A, Sigma) in culture medium for 3 h at 37 °C; the resulting cell suspension was passed through a 70 mm nylon cell strainer (Falcon/Becton Dickinson). The filtrate was then transferred to centrifuge tubes and spun at 300 ***g*** for 5 min and the resulting pellet was washed three times and resuspended in culture medium. Cells were plated in 75 cm^2 culture flasks at a density of 50×10^3 cells/ml, and fresh medium was added to them once every 3 days.

One week later, once 80–90% confluence was reached, the cells were harvested using 0.1% trypsin and 0.04% EDTA solution for 8 min at 37 °C and replated at density of 2×10^4 cells/cm^2. Medium was changed once every 2 days, and cells from passage 2 were used for proliferation studies. All experiments were repeated at least three times.

Count protocol for proliferation studies

Ovine chondrocytes were plated at density 2×10^4 cells/cm^2 in 8 cm^2 Petri dishes (Corning B.V. Life Sciences, Amsterdam, Netherlands). Each day, cells from three plates were harvested using 218 μl of 0.1% trypsin and 0.04% EDTA solution for 8 min at 37 °C. Action of trypsin was stopped with 436 μl of complete medium, and Petri dishes were washed with 436 μl of PBS. Then, cells were counted using a haemocytometer and histograms of cells' diameter distribution were measured electronically using a Coulter Counter (Beckman Coulter Inc., Miami, Florida, USA) in a total volume of 1.09 ml.

Phenotypic characterization of chondrocyte proliferation

For flow cytometric analysis, chondrocytes were plated at density 2×10^4/cm^2 in 55 cm^2 dishes (Corning). According to the method of Wang *et al.* (32), after 1 day and at the end of the culture, cells were harvested for flow cytometry with 1 mmol/l EDTA in HBSS without Ca^{2+}/Mg^{2+} for 30 min. Limitation of EDTA treatment is related to difficulty of dissociating confluent monolayer-cultured chondrocytes embedded in a dense matrix. Chondrocytes were therefore seeded in low-density cultures (5×10^3/cm^2) and phenotypes were defined after 4 days in subconfluent cultures. This procedure made it possible to obtain single cells embedded in a cell-associated matrix.

Cell aliquots (2×10^5/100 μl) were incubated for 3 min with propidium iodide to exclude dead cells, then two aliquots were incubated in 0.1% pepsin to unmask sites of collagen type I and type II; an aliquot was incubated with 0.01 units of keratanase and 0.01 units of chondroitinase ABC to unmask sites of aggrecan. After fixation with 4% PFA, cell aliquots were incubated for 30 min with monoclonal antibody (mAb) followed by two washing steps in PBS containing 0.1% BSA and again incubated with conjugated secondary antibody for 20 min at room temperature. Mouse monoclonal anti-aggrecan antibody (Novus Biologicals, Cambridge, UK), mouse anti-human type I and type II collagen monoclonal antibodies (Chemicon International, Millipore S.p.A., Milano, Italy) and secondary FITC-conjugated sheep F(ab′)2 fragment anti-mouse IgG antibody (Chemicon International, Millipore S.p.A., Vimodrone, Milano, Italy) were used. Flow cytometry was performed using a fluorescence activated cell sorter (BD FACSCalibur, BD Biosciences, Franklin Lakes, NJ, USA) and analysed using the CellQuest Pro software (BD Biosciences, CA, USA).

Mathematical modelling and numerical solution

Mathematical simulation, provided by suitable predictive models, represents an important tool to facilitate experiments, helping to determine optimal operating conditions and at the same time contributing to understanding

of biological mechanisms, which affect cell proliferation kinetics. The mathematical model used in the present study has been proposed recently in the literature (1). It describes cell proliferation and corresponding size distribution during culture in batch systems. Assuming spatially uniform cell mass distribution and neglecting cell death by apoptosis (which is relevant only in the case of apoptotic/necrotic cells), the model equations are summarized in Table 2. In particular, the population balance of the cell density distribution, $\psi(m, t)$, is represented by Eqn (1), along with the initial and boundary conditions (Eqns 2 and 3). Symbol's significance is reported in the list of abbreviations.

Table 2. Model equations

Mass-based population balance of chondrocytes

$$\frac{\partial \psi(m,t)}{\partial t} = -\frac{\partial [v\,\psi(m,t)]}{\partial m} + 2\int_m^{\infty} \psi(m',t)\,\Gamma^M(m', C_{O_2})\,p(m,m')\,dm' - \psi(m,t)\,\Gamma^M(m, C_{O_2}) \quad (1)$$

$$\psi(m,t) = \psi^0(m) \quad \text{for} \quad t = 0 \quad \text{and} \quad \forall\, m \quad (2)$$

$$\psi(m,t) = 0 \quad \text{for} \quad t > 0 \quad \text{and} \quad m = 0 \quad (3)$$

Partitioning distribution function

$$p(m,m') = \frac{1}{\beta(q,q)}\frac{1}{m'}\left(\frac{m}{m'}\right)^{q-1}\left(1-\frac{m}{m'}\right)^{q-1} \quad (4)$$

$$\beta(q,q) = \frac{(\Gamma(q))^2}{\Gamma(2q)} \quad (5)$$

$$\Gamma(q) = \int_0^{+\infty} s^{q-1}\,\mathrm{e}^{-s}\,ds. \quad (6)$$

Division rate function (mitosis kernel)

$$\Gamma^M(m, C_{O_2}) = v(m, C_{O_2}) \cdot \gamma^M(m) \quad (7)$$

$$\gamma^M(m) = \frac{f(m)}{1-\int_0^m f(m')dm'} \quad (8)$$

$$f(m) = \frac{1}{\sqrt{2\pi\sigma^2}}\exp\frac{-(m-\mu)^2}{2\sigma^2} \quad (9)$$

Cell mass growth rate

$$v(m, C_{O_2}) = \left(\frac{3}{d_c}\right)^{2/3}(4\pi)^{1/3}m^{2/3}\frac{\mu' C_{O_2}}{C_m + C_{O_2}}\Phi - \mu_c m \quad (10)$$

$$\Phi(t) = \left[1 - \frac{\varphi(t)}{\varphi_a}\right]^{\alpha_P} \quad (11)$$

$$\varphi = V\left(\frac{4}{\pi}\right)\left(\frac{3\pi}{4\,d_c}\right)^{2/3}\int_0^{\infty} m^{2/3}\,\psi(m,t)\,dm \quad (12)$$

Regression analysis functions

$$F = \sum_{i=1}^{8}\left[\frac{N_i^{\exp} - N_i^{\mathrm{calc}}}{N_i^{\exp}}\right]^2 + \sum_{i=1}^{4}\left[\frac{\sum_{j=1}^{100}\left(P_{c,i,j}^{\exp} - P_{c,i,j}^{\mathrm{calc}}\right)^2}{\sum_{j=1}^{100}\left(P_{c,i,j}^{\exp}\right)^2}\right] \quad (13)$$

$$N_i^{\mathrm{calc}} = V\int_0^{\infty}\psi(m,t_i)dm \quad (14)$$

$$P_{c,i,j}^{\mathrm{calc}} = 100\,\frac{V\psi(m_j,t_i)}{N_i^{\mathrm{calc}}}(m_{j+1} - m_j) \quad (15)$$

In Eqn (1), the left hand side represents accumulation; first term on the right hand side represents cell growth, second cell birth where two daughters cells are obtained by division of a larger mother cell, and third the corresponding removal of mother cell as a result of mitosis. In Eqn (2), $\psi^0(m)$ represents initial distribution of cells, and physical meaning of the boundary condition for the PBE model given by Eqn (3) is that there exist no cells of zero mass at any time (13).

The PBE model adopted is a single-variable, unstructured, single-staged PBE. Specifically, it considers cell mass as internal coordinate, as age-structured PBE models cannot be validated easily by comparison with experimental data. Unstructured and single-staged characteristics of the adopted PBE approach are aimed to minimize model complexity that reflects into lowering number of the adjustable parameters. Indeed, without distinguishing among cells belonging to different cell cycle phases and by neglecting complex intra- and extracellular biochemistry, the proposed model permits one to track the essential features of cell proliferation taking place and to simulate confluence limitation resulting from contact inhibition, when a saturation level is reached within the Petri dish (1).

The three generally unknown functionalities appearing in the mass-based PBE (1), namely cell mass growth (v), cell division rate (Γ^M) and partitioning distribution of mother cell into daughters (p) are adopted as reported in Table 2. Details may be found elsewhere (1). However, it is worth noting that cell mass m is used to predict cell division, and, specifically, it is assumed that probability of cell division is higher when cell mass reaches the particular value of μ (Eqn 9 in Table 2).

Mitotic rate Γ^M, as shown in Eqn (7), increases as growth rate v is augmented, which, on the other hand, is characterized by two terms (Eqn 10). The anabolic (positive) term for a single cell is proportional to its surface area ($m^{2/3}$), while the catabolic term (negative) is proportional to cell mass (m). In Eqn (10), limiting supply of oxygen (nutrient) is taken into account by classic Monod kinetics (11,21). However, as the experimental procedure adopted in this study guarantees constant concentration of nutrients supplied to the expanding culture, relevant oxygen material balance is not taken into account.

Contact inhibition, which progressively slows culture expansion when reaching confluence in the Petri dish as proliferation progresses, is simulated by a limiting factor ($\Phi(t) \leq 1$) appearing in the anabolic term of Eqn (10), and related to available superficial area between cells on the Petri dish surface, assuming that ovine chondrocytes distribute themselves in a monolayer.

Equation (1) is a partial differential equation in variables t and m along with the initial and boundary

conditions, Eqns (2) and (3), respectively. In particular, the mass domain of integration ranges from 0 to +∞, as in general, cells of any positive size (mass) may theoretically exist. This upper limit is obviously not tractable by numerical analysis. A relatively high but finite value may be safely chosen if cell distribution $\psi(m,t)$ is entirely contained in the resulting m domain. In this study, during its dynamic behaviour, the upper limit was chosen equal to 16 ng. The numerical solution of partial differential Eqn (1) along with initial and boundary conditions Eqns (2) and (3) is solved by means of the method of lines (33). After choice of the upper limit, the mass domain is divided using a constant step size mesh, and only the partial derivative with respect to m is discretized by backward finite difference. Thus, partial differential Eqn (1) is transformed into a system of ordinary differential equations in time, which is integrated by means of standard numerical libraries (Gear method, IMSL) as an initial value problem. One hundred grid points in the mass domain are typically used for numerically solving the PBE model, because finer grids have been shown to not provide significant improvements in accuracy. Details of the numerical method used and discretizing scheme have been reported elsewhere (1)**.**

The fitting procedure adopted for determining the unknown, adjustable model parameters consisted of minimizing cost function F (Eqn 13 of Table 2), where index i represents the generic culture day, j generic cell diameter position in the discretized cell size distribution, $N_i^{\exp}$ experimental total cell count, N_i^{calc} the calculated one, and, finally, $P_{c,i,j}^{\exp}$ and $P_{c,i,j}^{\text{calc}}$ experimental and calculated cell number percentages (histograms), respectively. At the generic time instant i-th, total number of cells, N_i^{calc}, and cell distribution, $P_{c,i,j}^{\text{calc}}$, are evaluated from knowledge of $\psi(m,\ t)$ as indicated in Eqns 14 and 15 of Table 2, respectively, where m_j is generic mass corresponding to generic (j-th) diameter of the experimental bin. Minimization of cost function F is carried out by means of standard numerical libraries (Optimization, IMSL).

Results and discussion

Phenotypic characterization of ovine chondrocytes was considered first. In particular, flow cytometric analyses performed for the seeded cells (at the initial time) and for cells harvested after long-term culture (17 days) are reported in Fig. 1. Only viable cells, determined using propidium iodide (PI) exclusion test (gate R3 in Fig. 1), were phenotypically characterized using markers for aggregan, and type I and II collagen.

When expanded in a monolayer culture, chondrocytes have been shown to lose their original phenotype and to de-differentiate to fibroblast-like cells. In particular, native chondrocytes produce primarily two structural macromolecules (aggrecan, a large, aggregating proteoglycan and type II collagen), which are then used to define their

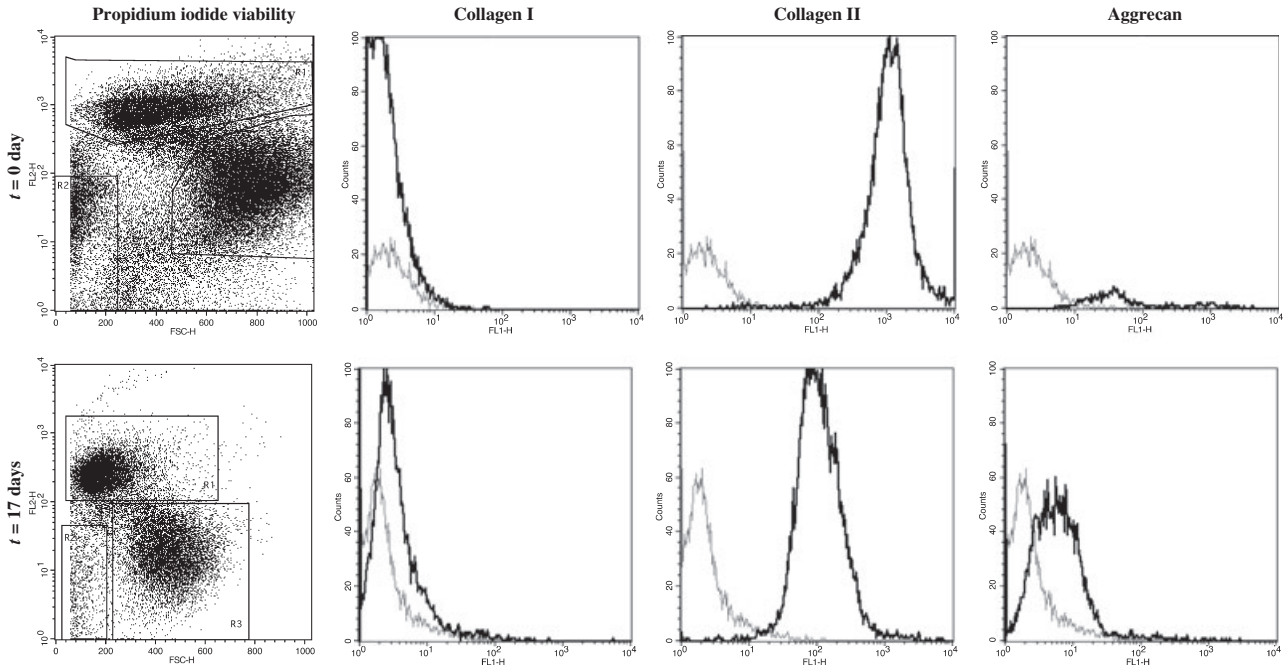

Figure 1. Viability and phenotypic characteristics of ovine chondrocytes at time 0 days and after 17 days of culture in Petri dishes. White area indicates isotypic control (cells without staining) and black indicates positive staining.

differentiated phenotype. However, when released from their extracellular matrix and placed into monolayer culture for expansion, mammalian chondrocytes are known to stop producing these characteristic macromolecules (34,35). Such chondrocytes are referred to as *dedifferentiated*, to emphasize loss of differentiated functions. Dedifferentiated chondrocytes are similar to fibroblasts and are characterized by a change in collagen secretion from type II to type I and by a decrease in aggrecan production. They also acquire a flattened, irregular shape, which is in contrast to the more rounded shape of differentiated chondrocytes.

As clearly reported in Fig. 1, viable seeded cells are negative and positive for type I collagen and both type II collagen and aggrecan, respectively. As this phenotypic expression is maintained after 17 days of culture, it may be safely concluded that chondrocytes considered in this study do not de-differentiate during long-term culture in Petri dishes, and thus, proliferation with monolayer tendency is the only biological phenomenon taking place during the performed experimental runs.

Initial cell distribution, measured using the electronic Coulter Counter (Beckman Dickinson) in terms of cell percentage (histogram) as a function of cell diameter (μm), is reported in Fig. 2. Distribution *mode* is placed at about 13.7 μm. To numerically solve the adopted model, this measured initial cell distribution has to be converted to number distribution density $\psi^0(m)$, considered in the initial condition [cf. Eqn (2) in Table 2]. To this aim, spherically shaped cells whose mass is given by $m = \frac{4}{3}\,\pi\,\left(\frac{d}{2}\right)^3 d_c$, where d and d_c are diameter and mass density of cells, respectively, were assumed. Starting from the experimental histogram $P^{\exp}_{c,0,j}$ reported in Fig. 2, the

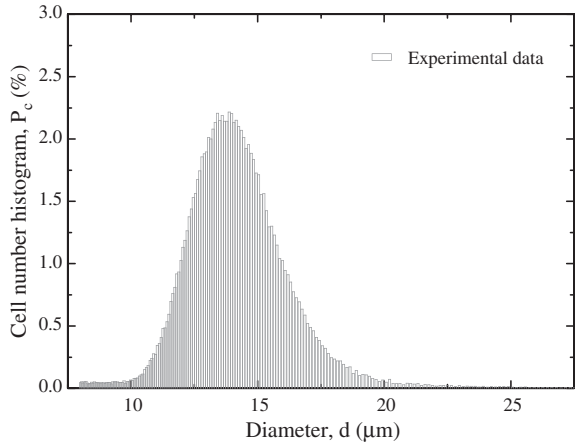

Figure 2. Experimental cell size distribution in terms of chondrocyte number percentage (histogram) as a function of cell diameter measured using the electronic Coulter Counter.

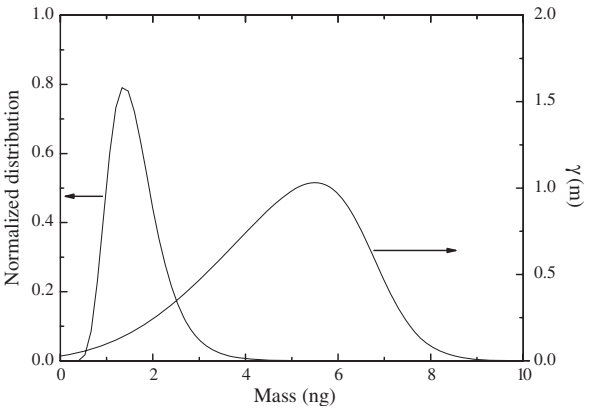

Figure 3. Initial, normalized cell mass density distribution and gamma function, $\gamma^M(m)$, used in simulations.

discretized version of initial cell mass number density distribution is readily obtained as

$$\psi^0(m_j) = \frac{N_0^{\exp}}{100 \cdot V} \cdot \frac{P^{\exp}_{c,0,j}}{(m_{j+1} - m_j)}.$$

Then, using quadratic interpolation, its corresponding continuous version was determined, so that its value at any grid point of the uniform mesh numerically adopted for solving the model by the method of lines, may be calculated. Normalized initial distribution, $\frac{V\psi_0(m)}{N_0^{\exp}}$, as well as the gamma function, $\gamma^M(m)$, defined in Eqn (8), used in simulations, is depicted in Fig. 3.

Table 3. Model parameters for PBE modelling approach used in the simulation. Parameters μ', μ_C, q, σ and α_P, are obtained by fitting model results against experimental data

Parameter	Value	Unit	Reference
μ_C	1.8×10^{-3}	1/h	This study (tuned parameter)
μ'	122.1	ng/(mm^2 h)	This study (tuned parameter)
σ	1.5	ng	This study (tuned parameter)
q	50	–	This study (tuned parameter)
α_P	10.1	–	This study (tuned parameter)
N^0	1.6×10^5	cells	This study (experimental condition)
V	800	mm^3	This study (experimental condition)
φ_a	800	mm^2	This study (experimental condition)
Co_2	0.203×10^{-6}	mmol/mm^3	Schumpe *et al.* (36)
C_m	0.006×10^{-6}	mmol/mm^3	Obradovic *et al.* (5)
d_c	1.14×10^6	ng/mm^3	Jakob *et al.* (37)
μ	3.2	ng	This study [assumed according to Mantzaris *et al.* (13)]

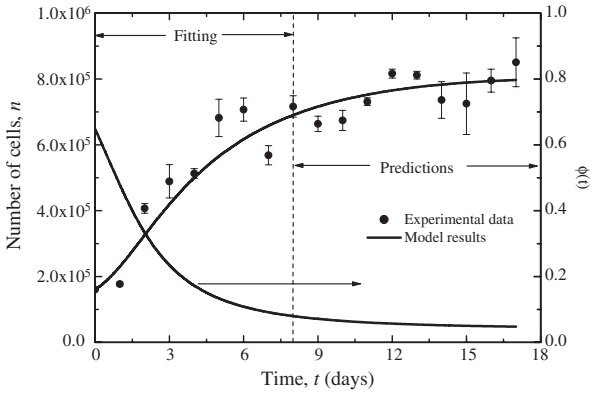

Figure 4. Comparison between model results and experimental data in terms of total chondrocyte count cultured in Petri dishes, starting with 1.6×10^5 cells. Data are expressed as mean ± standard deviation. Fitting is performed for culture time of up to 8 days. Temporal evolution of the geometric limiting factor $\Phi(t)$ defined by Eq. (11) of Table 2 is also plotted.

To determine the unknown model parameters by minimizing objective function defined in Eqn (13) of Table 2, model results were fitted to measured total cell count (up to 8 days of culture time) and cell distribution expressed as number percentage of cells (histogram) as a function of cell diameter (up to 4 days of culture time). Values of model parameters used in simulation runs are reported in Table 3. It is seen that some of them are taken from the literature, others are obtained by fitting to experimental data, while remaining ones represent operative conditions used experimentally in this study. In particular, mean of normal distribution of mitotic fraction [μ in Eqn (9) of Table 2] is assumed equal to about twice the value of the mode of measured initial distribution shown in Fig. 3 (μ = 3.2 ng = 2 x 1.6 ng). This seems a reasonable choice (13). As no synchronization by either physical or biochemical means was performed on the cell population, mode of the initial distribution should correspond to mean size of daughter cells (which are typically many more than

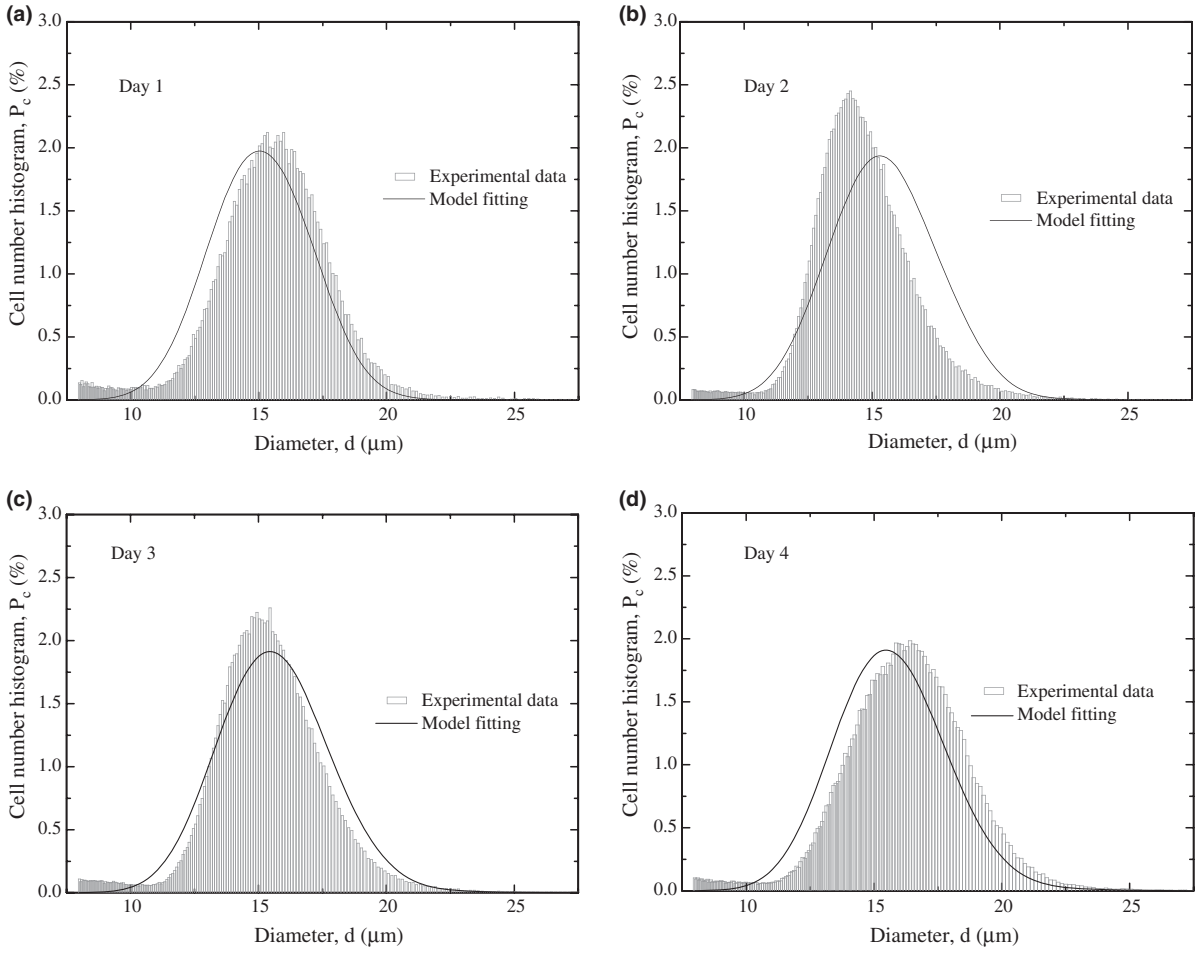

Figure 5. Comparison between model fitting and experimental data in terms of cell size distribution (cell percentage as a function of diameter, histogram) at different culture times: 1 (a), 2 (b), 3 (c) and 4 days (d).

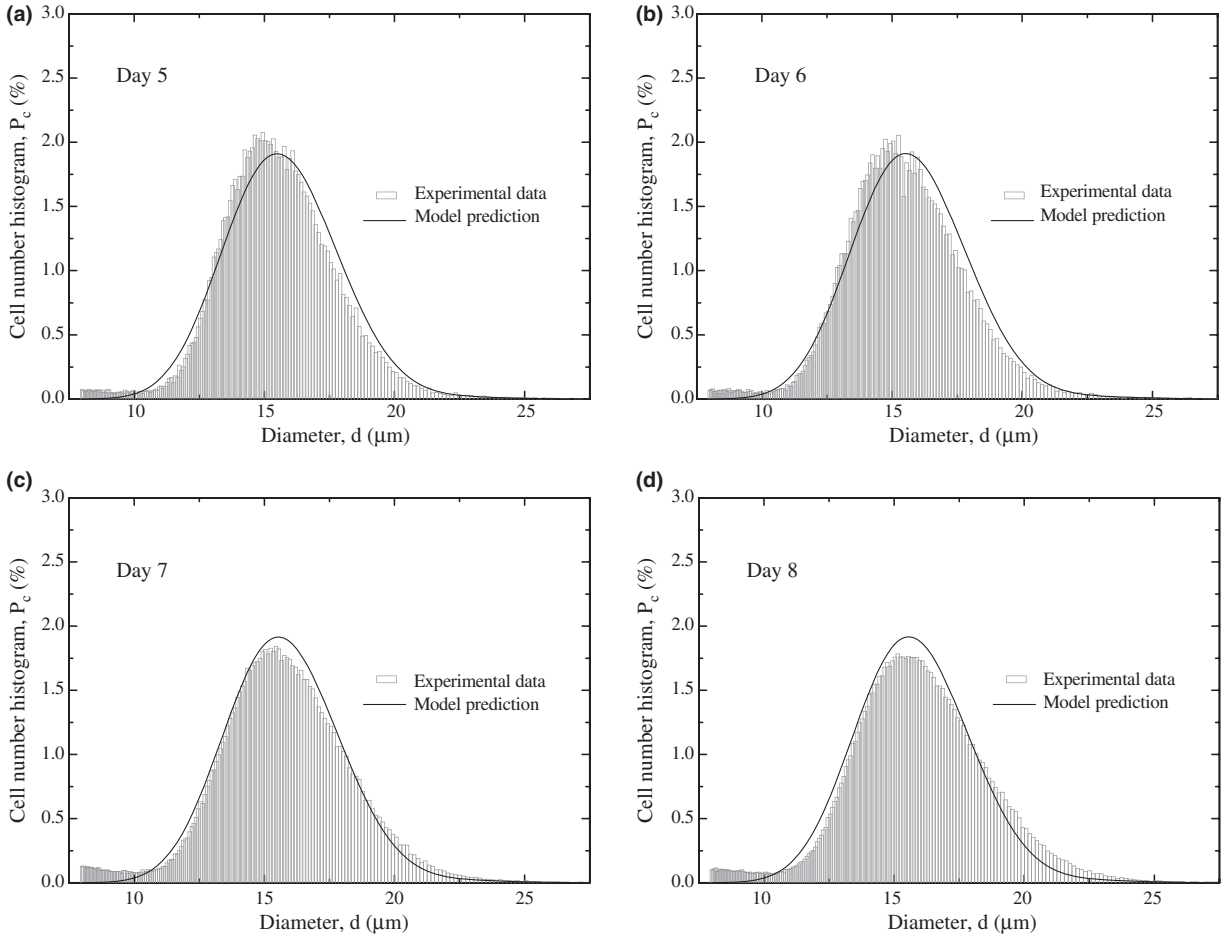

Figure 6. Comparison between model predictions and experimental data in terms of cell size distribution (cell percentage as a function of diameter, histogram) at different culture times: 5 (a), 6 (b), 7 (c) and 8 days (d).

any other cell of S or G_2/M cell cycle phases). Five parameters were determined using a non-linear fitting procedure: proportionality constant, μ', of cell mass rate, catabolic constant, μ_C, order α_P of the power law given in Eqn (11) of Table 2, parameter q of the partitioning function, and σ, value of variance of normal distribution on mitotic fraction appearing in Eqn (9) of Table 2. Comparison between model results and experimental data in terms of total cell number as a function of culture time is depicted in Fig. 4 along with geometric limiting factor $\Phi(t)$, while in Figs 5–7, comparisons in terms of cell percentage distributions (histograms) as a function of cell diameter are reported. The relative error obtained by the fitting procedure is equal to around 16%, and values of fitted model parameters are reported in Table 3. Good agreement between model results and experimental data demonstrate validity of the proposed modelling approach. In particular, the model's predictive capability is displayed at culture times longer than 4 days for cell distribution (Figs 6 and 7) and after 8 days for total cell count data (Fig 4). According to the adopted mathematical model, when seeding density is equal to 2×10^4 cells/cm^2, as a result of contact inhibition, chondrocyte proliferation in the Petri dish slows and essentially stops after 10 days in culture. This occurs when $\Phi(t)$ almost reaches its lowest value, as depicted in Fig. 4, thus limiting cell mass growth and mitotic rates, v and Γ^M, respectively.

In particular, significant overlapping between initial cell and $\gamma^M(m)$ distributions (Fig. 3) indicates presence of a mitotic fraction in the cell population, seeded into the Petri dish. According to the adopted model, initially the cell population gains weight to reach a mitotic size, thus showing short induction time before proliferation begins. This is confirmed by the temporal profile of total counts reported in Fig. 4, whose slope starts slowly, and by shifting of cell distribution towards sizes higher than those measured initially at seeding (Figs 2 and 5a). This behaviour may be more easily recognized from the analysis of Fig. 8, where the complete (up to reaching of confluence) evolution of the modelled size distributions

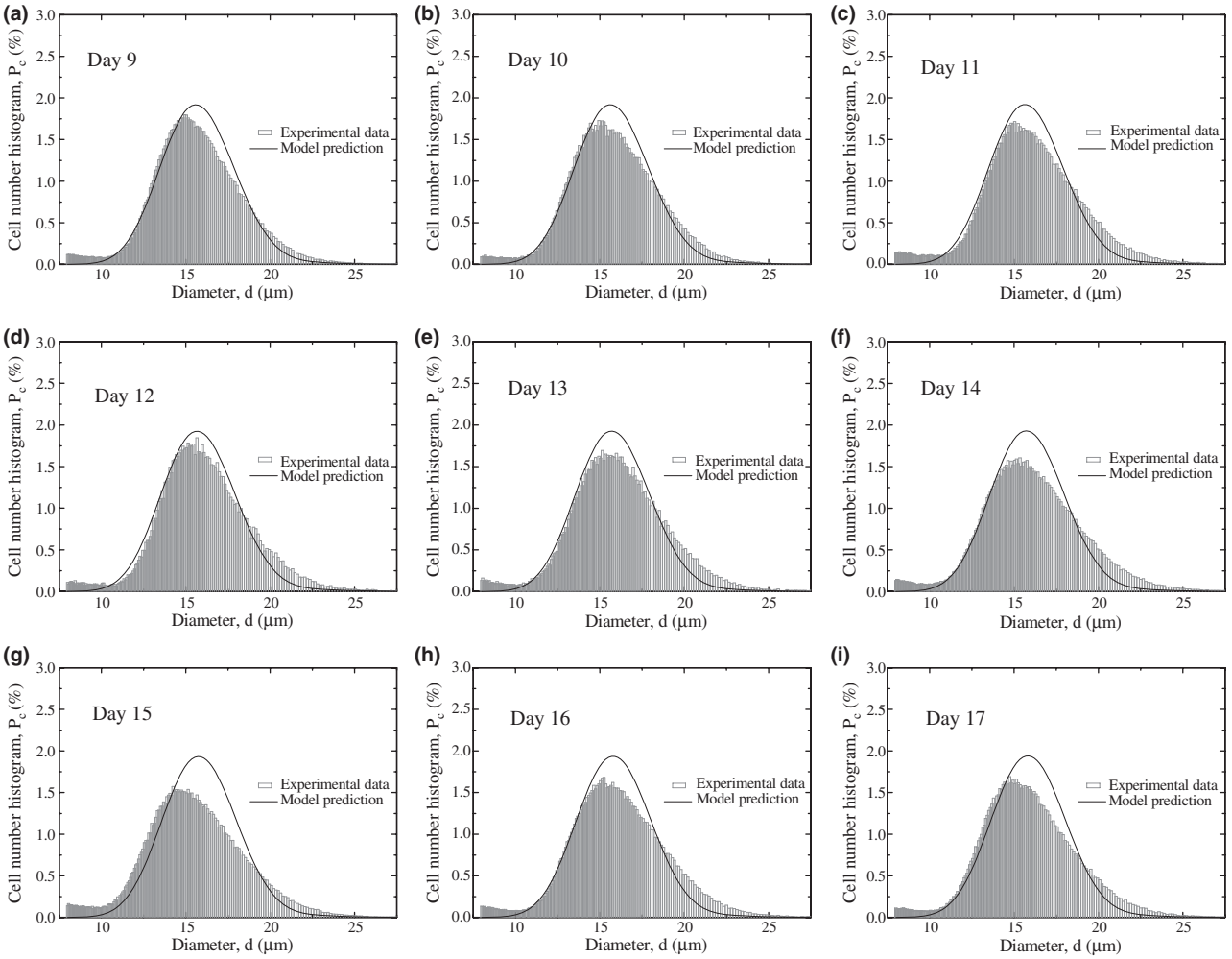

Figure 7. Comparison between model predictions and experimental data in terms of cell size distribution (cell percentage as a function of diameter, histogram) at different culture times: 9 (a), 10 (b), 11 (c), 12 (d), 13 (e), 14 (f), 15 (g), 16 (h), and 17 days (i).

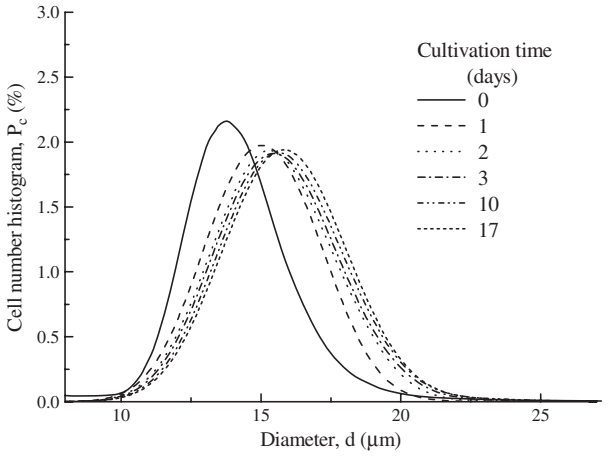

Figure 8. Evolution of modelled cell size distribution (cell percentages as a function of diameter, histograms) at different culture times.

during long-term culture is reported, without comparison with the measured experimental data, for the sake of clarity.

The proposed model is not able to perfectly interpret measured transient behaviour, which takes place during the first 2 days of culture. Indeed, as illustrated in Fig. 5, measured cell distribution displays a transient behaviour, which seems to move back and forth as mitosis and growth take place (distribution mode at the beginning shifts towards larger values, $t = 1$ days, and successively to lower values, $t = 2$ days). However, after the third day of culture, cell proliferation behaviour becomes regular and the model interprets typical 'balanced growth' condition well, where normalized number distribution of a cell population reaches a time-invariant condition (Fig. 8). Then, good model predictions for cell size distributions are obtained at intermediate culture times, as reported in

Fig. 6. At longer culture times, on the contrary (cf. Fig. 7), model predictions of cell size distributions progressively worse. In particular, measured cell sizes are shifted towards lower values than those calculated using the adopted model. This is presumably due to ECM deposition by chondrocytes, which increases as culture progresses. Indeed, harvesting attached cells using trypsin may generate a relatively high number of small pieces of debris when ECM production reaches a relevant level, thus negatively affecting Coulter Counter measurements, as electrical sensing zone does not allow discrimination between cells and any other material. In principle, this hypothesis could have been partly confirmed by cytofluorimetric analysis through which stained cells and debris can be discriminated. Indeed, it would be possible to count (through gating) increasing percentage of debris formed when using trypsin due to the increased ECM deposition as culture proceeds, although without quantifying the effect of presence of debris on cell size distributions. On the other hand, the hypothesis could have been partly confirmed also by experimentally evaluating increasing GAG concentration temporal profile inside the Petri dish. In addition, this would allow determination of ECM deposition kinetics. From the modelling perspective, this task could be accomplished easily by accounting for a specific material balance equation for GAG in the model, similar to that used in previous studies (cf. 24–26). An attempt was made to measure GAG through spectrophotometric analysis. In particular, the 1,9-dimethylmethylene blue (DMMB) assay described by Farndale *et al.* (38) has been adopted, but, unfortunately, experimental data obtained were discarded due to lack of an adequate experimental reproducibility.

Conclusion

Mathematical modelling and simulation of proliferation kinetics and cell size distribution of chondrocytes of ovine articular cartilage expanded up to confluence in Petri dishes is addressed in this study. The sigmoidal temporal profiles of total counts and cell size distribution were quantitatively interpreted by a 1-D population balance model, which is able to take into account contact inhibition at confluence. The proposed population balance modelling approach has been successful in predicting proliferation kinetics in terms of cell count and size distribution, thus contributing towards quantitative interpretation of the *in vitro* cell proliferation.

Study is in progress for extending experimental validation of the proposed model, which can be (in our view) easily applied to the case of human cells, where specific values of model parameters change accordingly to such a cell lineage.

Acknowledgements

We gratefully acknowledge the financial support by Ministero dell'Università e della Ricerca (MIUR), Italy through the project PRIN 2006 'Bioreattori per l'ottimizzazione dei segnali biochimici nella ingegnerizzazione di tessuto cartilagineo e osseo'. We also thank BT (Biomedical Tissues) Srl for permitting the use of Coulter Counter.

References

1 Mancuso L, Liuzzo MI, Fadda S, Pisu M, Cincotti A, Arras M *et al.* (2009) Experimental analysis and modeling of in vitro mesenchymal stem cells proliferation. *Cell Prolif.* **42**, 602–616.
2 Freed LE, Vunjak-Novakovic G (1995) Tissue engineering of cartilage. In: Bronzino JD, ed. *The Biomedical Engineering Handbook*, chapter 120, pp. 1788–1806. Boca Raton, Florida, USA: CRC Press.
3 Freed LE, Martin I, Vunjak-Novakovic G (1999) Frontiers in tissue engineering: in vitro modulation of chondrogenesis. *Clin. Orthop. Relat. Res.*, **15**, 682.
4 Munteanu SE, Ilic MZ, Handley CJ (2002) Highly sulfated glycosaminoglycans inhibit aggrecanase degradation of aggrecan by bovine articular cartilage explant culture. *Matrix Biol.* **21**, 429–440.
5 Obradovic B, Meldon JH, Freed LE, Vunjak-Novakovic G (2000) Glycosaminoglycan deposition in engineered cartilage: experiments and mathematical model. *AIChE J.* **46**, 1860–1871.
6 Wilson CG, Bonassar LJ, Kohles SS (2002) Modeling the dynamic composition of engineered cartilage. *Arch. Biochem. Biophys.* **408** (2), 246–254.
7 Zhou S, Cui Z, Urban JPG (2004) Factors influencing the oxygen concentration gradient from the synovial surface of articular cartilage to the cartilage-bone interface. A modeling study. *Arthritis Rheum.* **50**, 3915–3924.
8 Deasy BM, Jankowski RJ, Payne TR, Cao B, Goff JP, Greenberger JS *et al.* (2003) Modeling stem cell population growth: incorporating terms for proliferative heterogeneity. *Stem Cells* **21**, 536–545.
9 Kozusko F, Bourdeau M (2007) A unified model of sigmoid tumour growth based on cell proliferation and quiescence. *Cell Prolif.* **40**, 824–834.
10 de Vladar HP (2006) Density-dependence as a size-independent regulatory mechanism. *J. Theor. Biol.* **238**, 245–256.
11 Eakman JM, Fredrickson AG, Tsuchiya HM (1966) Statistics and dynamics of microbial cell populations. *Bioeng. Food Process.* **62**, 37–49.
12 Liou J-J, Srienc F, Fredrickson AG (1997) Solutions of population balance models based on a successive generations approach. *Chem. Eng. Sci.* **52**, 1529–1540.
13 Mantzaris NV, Liou JJ, Daoutidis P, Srienc F (1999) Numerical solution of a mass structured cell population balance in an environment of changing substrate concentration. *J. Biotechnol.* **71**, 157–174.
14 Abu-Absi N, Srienc F (2002) Instantaneous evaluation of mammamlian cell culture growth rates through the analysis of the mitotic index. *J. Biotechnol.* **95**, 63–84.
15 Cipollina C, Vai M, Porro D, Hatzis C (2007) Towards understanding of the complex structure of growing yeast populations. *J. Biotechnol.* **128**, 393–402.
16 Mantzaris N (2006) Stochastic and deterministic simulations of heterogeneous cell population dynamics. *Journal of Theoretical Biology.* **241**, 690–706.

17 Sherer E, Tocce E, Hannemann RE, Rundell AE, Ramkrishna D (2008) Identification of age-structured models: cell cycle phase transitions. *Biotechnol. Bioeng.* **99**, 960–974.
18 Sidoli FR, Asprey SP, Mantalaris A (2006) A coupled single cell-population model for mammalian cell cultures. *Ind. Eng. Chem. Res.* **45**, 5801–5811.
19 Hatzis C, Srienc F, Fredrickson AG (1995) Multistaged corpuscolar models of microbial growth: Monte Carlo simulations. *Biosystems* **36**, 19–35.
20 Basse B, Baguley BC, Marshall ES, Wake GC, Wall DJN (2004) Modelling cell population growth with applications to cancer therapy in human tumour cell lines. *Prog. Biophys. Mol. Biol.* **85**, 353–368.
21 Liu Y-H, Bi J-X, Zeng A-P, Yuan J-Q (2007) A population balance model describing the cell cycle dynamics of myeloma cell cultivation. *Biotechnol. Prog.* **23**, 1198–1209.
22 Busini V, Arosio P, Masi M (2007) Mechanistic modelling of avascular tumor growth and pharmacokinetics influence-Part I. *Chem. Eng. Sci.* **62**, 1877–1886.
23 Hatzis C, Porro D (2006) Morphologically-structured models of growing budding yeast populations. *J. Biotechnol.* **124**, 420–438.
24 Pisu M, Lai N, Cincotti A, Delogu F, Cao G (2003). A simulation model for the growth of engineered cartilage on polymeric scaffolds. *Int. J. Chem. Reactor Eng.*. http://www.bepress.com/ijcre/vol1/A38.
25 Pisu M, Lai N, Cincotti A, Concas A, Cao G (2004) Model of engineered cartilage growth in rotating bioreactors. *Chem. Eng. Sci.* **59**, 5035–5040.
26 Pisu M, Concas A, Lai N, Cao G (2006) A novel simulation model for engineered cartilage growth in static systems. *Tissue Eng.* **12**, 2311–2320.
27 Schultze-Tanzil G, Müller RD, Kohl B, Schneider N, Ertel W, Ipaktchi K *et al.* (2008) Differing in vitro biology of equine, ovine, porcine and human articular chondrocytes derived from knee joint: an immunomorphological study. *Histochem. Cell Biol.* **131**, 219–229.
28 Stewart K, Pabbruwe M, Dickinson S, Sims T, Hollander AP, Chaudhuri JB (2007) The effect of growth factor treatment on meniscal chondrocyte proliferation and differentiation on polyglycolic acid scaffolds. *Tissue Eng.* **13**, 271–280.
29 Akens MK, Hurting MB (2005) Influence of species and anatomical location on chondrocyte expansion. *BMC Musculoskelet. Disord.* **6**, 23.
30 Schulz RM, Zscharnack M, Hanisch I, Geiling M, Hepp P, Bader A (2008) Cartilage tissue engineering by collagen matrix associated bone marrow derived mesenchymal stem cells. *Biomed. Mater. Eng.* **18**(1 Suppl), 55–70.
31 Fuchs JR, Hannouche D, Terada S, Zand S, Vacanti JP, Fauza DO (2005) Cartilage engineering from ovine umbilical cord blood mesenchymal progenitor cells. *Stem Cells* **23**, 958–964.
32 Wang L, Verbruggen G, Almqvist KF, Elewaut D, Broddelez C, Veys EM (2001) Flow cytometric analysis of the human articular chondrocyte phenotype in vitro. *Osteoarthritis Cartilage* **9**, 73–84.
33 Schiesser WE (1991). *The Numerical Method of Lines*. San Diego, California, USA: Academic Press.
34 Pacifici M, Boettiger D, Roby K, Holtzer H (1977) Transformation of chondroblasts by Rous sarcoma virus and synthesis of the sulfated proteoglycan matrix. *Cell* **11**, 891–899.
35 Benya PD, Shaffer J (1982) Dedifferentiated chondrocytes reexpress the differentiated collagen phenotype when cultured in agarose gels. *Cell* **30**, 215–224.
36 Schumpe A, Quicker G, Deckwer DW (1982) Gas solubilities in microbial culture media. *Adv. Biochem. Eng.* **24**, 1–38.
37 Jakob M, Démarteau O, Schäfer D, Stumm M, Heberer M, Martin I (2003) Enzymatic digestion of adult human articular cartilage yields a small fraction of the total available cells. *Connect. Tissue Res.* **44**, 173–180.
38 Farndale RW, Sayers CA, Barrett AJ (1982) A direct spectrophotometric microassay for sulfated glycosaminoglycans in cartilage cultures. *Connect. Tissue Res.* **9**, 247–248.

Abbreviations:

C_{O_2}	concentration of O_2 at saturation condition, mmol/mm^3
C_m	oxygen concentration at half-maximal consumption, mmol/mm^3
d	cell diameter, μm
d_c	mass density, ng/mm^3
$f(m)$	division probability density function, 1/ng
m	single cell mass, ng
m'	mother cell mass, ng
N	cell number, cells
P_c	cell number percentage
P	partitioning function
Q	coefficient appearing in symmetric beta function
T	time, d
V	total culture volume, mm^3
Greek symbols	
α_P	order of the power law given in Eq. (11)
$\beta(q,q)$	symmetric beta function
φ	occupied area by cells and interstices, cm^2
φ_a	Petri dish area, cm^2
Φ	geometric limiting factor
$\Gamma(q)$	gamma function
γ^M	distribution defined in Eq. (8), 1/ng
Γ^M	division rate function, 1/d
M	average mass of dividing cells in Eq. (9), ng
μ'	maximum rate of cell growth, ng/(cm^2 h)
μ_c	catabolic rate, 1/h
v	time rate of change of cell mass m, ng/h
σ	standard deviation of the Gaussian distribution f(m) defined in Eq. (9), ng
ψ	cell distribution function, cells/(ng mm^3)